

# On the Kinetic Interpretation of DFT-Derived Energy Profiles: Cu-Catalyzed Methanol Synthesis

Werner Janse van Rensburg · Melissa A. Petersen ·  
Michael S. Datt · Jan-Albert van den Berg ·  
Pieter van Helden

Received: 12 September 2014 / Accepted: 21 October 2014 / Published online: 5 November 2014  
© Springer Science+Business Media New York 2014

**Abstract** A mean field microkinetic evaluation of previously reported DFT-derived Gibbs free energy profiles for CO and CO<sub>2</sub> hydrogenation to methanol on Cu(111), Cu(211) and Zn-modified Cu(211) is presented. It is demonstrated that explicit consideration of the effect of surface coverages of reaction intermediates on rates is needed in order to arrive at a realistic evaluation of the activity and selectivity. In particular, both the methanol formation rate and the CO/CO<sub>2</sub> selectivity for methanol production are demonstrated to be highly sensitive to the saturation coverage of formate at steady state. In general, the study emphasises the importance of including explicit kinetic analyses when mechanistic DFT-derived energy profiles are interpreted for catalytic processes.

**Keywords** Methanol synthesis · DFT · Copper · Microkinetic analysis · Mechanism

Commercial methanol synthesis from CO and CO<sub>2</sub> hydrogenation using Cu/ZnO/Al<sub>2</sub>O<sub>3</sub> catalysts [1] is considered to be one of the most important industrial catalytic processes [2]. Considerable interest towards the fundamental understanding of this catalytic process is reflected in the large number of density functional theory (DFT) studies published over the last 5 years that provide insight into the mechanism, catalyst models and kinetics. Whereas

most mechanistic computational studies focus on the direct interpretation of DFT-derived energy profiles [3–10], some studies also include kinetic evaluations of the DFT data [11–14]. The direct interpretation of DFT energies and mechanistic profiles provides for a qualitative description of elementary step reaction intermediates and relative energies, but is not necessarily sufficient to reliably assess the relative activities and selectivities inherent to the catalytic process. In the current contribution it is argued that explicit kinetic evaluation of DFT energy profiles is required in order to arrive at a reliable assessment of the rate and selectivity of the elementary reactions describing a catalytic process, as demonstrated using the example of Cu-catalyzed methanol synthesis.

Behrens et al. [9] showed that Zn-containing catalysts have a significantly higher intrinsic reactivity compared to a reference Cu catalyst sample for Cu/ZnO-catalyzed methanol synthesis. From neutron diffraction experiments a relatively high abundance of defects was established on the Cu nanoparticles, the formation of which manifests itself as local steps on the particle surface. From aberration corrected high resolution transmission electron microscopy (HRTEM) analysis on the most active catalyst sample a number of steps similar to those exposed on Cu(211) and Cu(522) surfaces were observed. In order to probe both the role of steps and the close proximity of Cu and Zn in the catalysts, Cu(111), Cu(211) and Zn-modified Cu(211) [designated as CuZn(211)] were utilized as model surfaces for mechanistic DFT studies. Two methanol synthesis sequences (based on the eleven unique elementary steps in Table 1) involving the hydrogenation of either CO or CO<sub>2</sub> were considered in the DFT studies. It is evident that some elementary reactions are shared by both sequences (i.e. reactions 2, 5 and 6), resulting in the formation of common intermediates during the hydrogenation of CO and CO<sub>2</sub>.

**Electronic supplementary material** The online version of this article (doi:10.1007/s10562-014-1407-1) contains supplementary material, which is available to authorized users.

W. Janse van Rensburg (✉) · M. A. Petersen ·  
M. S. Datt · J.-A. van den Berg · P. van Helden  
R&D Division, Sasol Technology (Pty) Ltd, 1 Klasie Havenga  
Road, Sasolburg 1947, South Africa  
e-mail: werner.jansevanrensburg@gmail.com

**Table 1** Elementary steps for methanol synthesis via CO and CO<sub>2</sub> hydrogenation considered in the studies of Behrens et al. [9], and Studt et al. [10]

Reaction	Number
CO Hydrogenation:	
CO(g) + * → CO*	(1)
H <sub>2</sub> (g) + 2* → 2 H*	(2)
CO* + H* → HCO* + *	(3)
HCO* + H* → H <sub>2</sub> CO* + *	(4)
H <sub>2</sub> CO* + H* → H <sub>3</sub> CO* + *	(5)
H <sub>3</sub> CO* + H* → H <sub>3</sub> COH(g) + 2*	(6)
CO <sub>2</sub> Hydrogenation:	
H <sub>2</sub> (g) + 2* → 2 H*	(2)
CO <sub>2</sub> (g) + H* → HCOO*	(7)
HCOO* + H* → HCOOH <sup>#</sup> + x*	(8)
HCOOH <sup>#</sup> + H* → H <sub>2</sub> COOH*	(9)
H <sub>2</sub> COOH* + * → H <sub>2</sub> CO* + OH*	(10)
H <sub>2</sub> CO* + H* → H <sub>3</sub> CO* + *	(5)
H <sub>3</sub> CO* + H* → H <sub>3</sub> COH(g) + 2*	(6)
OH* + H* → H <sub>2</sub> O(g) + 2*	(11)

\* Represents adsorbed states

# Represents gas phase in Ref [9] and adsorbed state in Ref [10];  
 x = 1 for adsorbed HCOOH and x = 2 for gas phase HCOOH

The DFT-calculated [9] non-standard Gibbs free energies ( $T = 500$  K,  $P$  of 40 bar for H<sub>2</sub>, 10 bar for CO and CO<sub>2</sub> and 1 bar of methanol and H<sub>2</sub>O), associated with the elementary reactions listed in Table 1, are illustrated as two profiles in Fig. 1 for CO and CO<sub>2</sub> hydrogenation, respectively. Hydrogenation sequences on each of the Cu(111), Cu(211) and CuZn(211) surfaces are presented on the same scale. It was noted [9] that the stability of both intermediates and transition states increase upon moving from flat Cu(111) to stepped Cu(211), with further stabilization incurred upon moving from stepped Cu(211) to CuZn(211), effectively suggesting increased catalytic activity according to the sequence: CuZn(211) > Cu(211) > Cu(111). This correlation of experimental results with calculated DFT data is put forward to explain observed catalyst activities and the nature of active sites for MeOH synthesis at a fundamental level.

Closer inspection of the CO hydrogenation energy profiles in Fig. 1a reveals that a major difference between the surfaces is the difference in the adsorption energies of CO and H<sub>2</sub>. Formation of CO\* and H\* on Cu(111) is endergonic by 0.33 and 0.30 eV, respectively, compared to corresponding endergonic values of only 0.09 and 0.14 eV on both the Cu(211) and CuZn(211) surfaces. Similarly for CO<sub>2</sub> hydrogenation in Fig. 1b, the more favourable interaction of CO<sub>2</sub> and H<sub>2</sub> with Cu(211) and CuZn(211) is reflected in the relatively more favourable reaction energies for formate formation, i.e. 0.06 and -0.06 eV respectively, compared to 0.57 eV on the Cu(111) surface. In order to

assess and quantify the significance of gas phase adsorption energies in controlling the relative reactivity of the Cu(111), Cu(211) and CuZn(211) surfaces, a microkinetic analysis of the DFT data is required.

All microkinetic analyses were performed within the mean-field approach [15] using the in-house developed *kinsolv* code [16]. DFT-based Gibbs free energy data were extracted <sup>1</sup> directly from the figures in the respective Behrens et al. [9] and Studt et al. [10] papers. Steady state concentrations and methanol synthesis rates are obtained from integration of the differential rate expressions and deriving rate constants from transition state theory

according to  $k = \left(\frac{k_B T}{h}\right) e^{-\Delta G_0^\ddagger/RT}$ , with  $k$  the rate constant,  $k_B$  Boltzmann's constant,  $h$  Planck's constant,  $T$  temperature,  $\Delta G_0^\ddagger$  activation free energy and  $R$  molar gas constant. For each of the surfaces studied, the microkinetic analyses consider the whole monolayer of catalyst sites to be represented by the respective energy profiles in Fig. 1. Table 2 presents steady state methanol formation rates for isolated CO hydrogenation, isolated CO<sub>2</sub> hydrogenation and combined CO and CO<sub>2</sub> hydrogenation based on the Gibbs free energy profiles in Fig. 1.

In Table 2 the methanol formation rates for isolated CO hydrogenation suggest a reactivity sequence of CuZn(211) > Cu(211) ≫ Cu(111), which is similar to previous predictions [9]. The slow methanol formation rate for Cu(111) could be attributed to the low coverage of both CO\* and H\* on the surface, presumably caused by the significantly endergonic nature of CO and H<sub>2</sub> adsorption on this surface. The more favourable adsorption of CO and H<sub>2</sub> on the Cu(211) and CuZn(211) surfaces yield CO\* and H\* steady state coverages of ~0.50 and ~0.10 ML, respectively. This results in methanol formation rates for Cu(211) and CuZn(211) which are in fair agreement with rates reported previously in single crystal studies upon increase in CO partial pressure in a CO/CO<sub>2</sub> feedstock [17]. The determining role played by CO and H<sub>2</sub> adsorption energies, in controlling the methanol formation rates on the different surfaces, is not only reflected in the significantly slower methanol formation rate for Cu(111), but also in the relatively similar rates observed for the Cu(211) and CuZn(211) surfaces. Notwithstanding the significantly lower relative free energies for most intermediates and transition states for CuZn(211) compared to the Cu(211) surface in Fig. 1a, the methanol formation rate on CuZn(211) is only found to be about two times faster. This supports the notion that the methanol formation rate is mainly determined by the steady state concentrations of CO\* and H\*, which are similar for CuZn(211) and Cu(211) at steady state. This suggests that the microkinetic surface

<sup>1</sup> See Supplementary Material for more information.

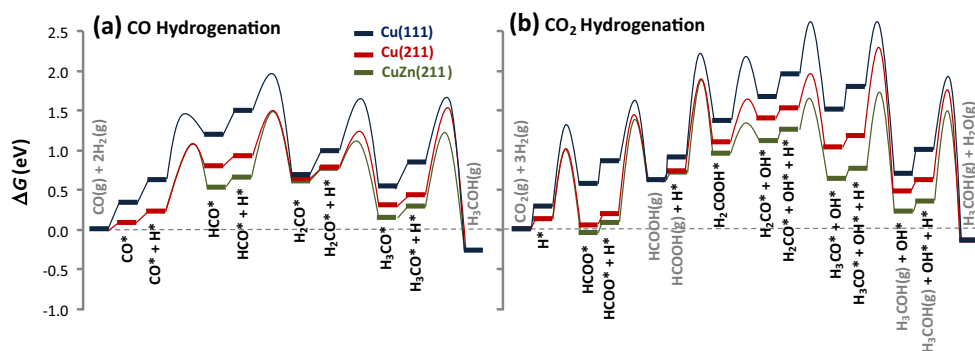


**Fig. 1** Representations of DFT-calculated Gibbs free energy [15] (non-standard) diagrams (500 K,  $P_{\text{H}_2} = 40$  bar,  $P_{\text{CO}} = P_{\text{CO}_2} = 10$  bar and  $P_{\text{MeOH}} = P_{\text{H}_2\text{O}} = 1$  bar) for methanol synthesis from **a** CO

hydrogenation and **b**  $\text{CO}_2$  hydrogenation on the Cu(111), Cu(211) and CuZn(211) surfaces, as reported by Behrens et al. [9]

reactivity trend is less a result of relative intermediate stability trends in the DFT energy profiles and more a result of the relative ability of the different surfaces to adsorb CO and  $\text{H}_2$  from the gas phase.

For the microkinetic study of  $\text{CO}_2$  hydrogenation in Table 2 two different treatments of gas phase formic acid were considered, which are indicated as *Analysis 1* and *Analysis 2*. For *Analysis 1* the formic acid pressure was constrained to zero bar in the microkinetic model, while for *Analysis 2* a low formic acid pressure (of the order of  $\sim 0.28$  mbar) was maintained in the models such that the production of formic acid at steady state corresponds to approximately 1 % of the methanol produced from  $\text{CO}_2$  consumption.<sup>2</sup> This is justified by the fact that MeOH selectivity is typically  $>99\%$ , effectively making a 1 % selectivity for formic acid an upper bound. *Analysis 1* of the methanol formation rates (Table 2) for  $\text{CO}_2$  hydrogenation in isolation shows no methanol formation for the three surfaces considered (instead, negligible methanol consumption, caused by the specified 1 bar pressure of

methanol in the kinetic analysis, is observed). The relatively favourable  $\text{CO}_2$  and  $\text{H}_2$  consumption rates are exclusively associated with formic acid formation (as to be expected given the definition of gas phase formic acid pressure for *Analysis 1*) according to the following reactivity trend:  $\text{Cu}(111) > \text{Cu}(211) > \text{CuZn}(211)$ . The higher activity of Cu(111) for formic acid formation is explained by the relatively high intrinsic rate for formate hydrogenation (i.e. lower direct barrier) to formic acid despite the low formate concentration on this surface. In contrast, the relative higher stability of formate on the Cu(211) and CuZn(211) surfaces, combined with significantly higher direct formate hydrogenation barriers, result in formate acting as a thermodynamic sink on these surfaces. This is reflected in the high steady state formate coverages obtained from the microkinetic analyses (vide infra). For more realistic <sup>3</sup> *Analysis 2* for isolated  $\text{CO}_2$  hydrogenation, the introduced formic acid gas phase pressures ensure the reincorporation of formic acid into the mechanism and yields a reactivity trend of  $\text{Cu}(211) > \text{CuZn}(211) \gg \text{Cu}(111)$  for methanol formation. Whereas the methanol formation rate on Cu(211) is found to be almost two times faster compared to CuZn(211), a two order slower rate on Cu(111) mirrors the reactivity trend observed for isolated CO hydrogenation amongst the three surfaces. This follows from the higher direct formic acid hydrogenation barrier on Cu(111) compared to Cu(211) and CuZn(211) in Fig. 2b. However, methanol formation from  $\text{CO}_2$  hydrogenation is consistently more than two orders of magnitude slower compared to methanol from CO hydrogenation on all three surfaces, effectively pointing towards a dominant selectivity for CO to produce methanol on all three surfaces (vide infra).

Due to the presence of common intermediates in the mechanisms for CO and  $\text{CO}_2$  hydrogenation (Table 1), the microkinetic analysis for combined CO and  $\text{CO}_2$  hydrogenation may readily be studied. This provides for a more

<sup>2</sup> Given that experimental Cu-catalyzed MeOH synthesis selectivity is  $>99\%$ , it is reasonable to assume that selectivity towards formic acid as product will not exceed 1 %. Therefore, the formic acid pressures associated with 1 % formic acid production in the kinetic runs were determined and found to be of the order of 0.28 mbar for all  $\text{CO}_2$  hydrogenation cases considered. *Analysis 2* runs thus treat this formic acid pressure as a fixed kinetic model input parameter essential in ensuring the reincorporation of formic acid into the mechanism for methanol production. Furthermore, the formic acid pressure is required to be relatively low to ensure that both formic acid and methanol are produced from  $\text{CO}_2$  hydrogenation, rather than the production of  $\text{CO}_2$  and methanol from the consumption of externally introduced formic acid. From an experimental perspective this approach is regarded as a more accurate kinetic treatment of  $\text{CO}_2$  conversion via formic acid to methanol compared to *Analysis 1* where no formic acid pressure build-up is allowed, artificially inhibiting the formation of methanol. Further validity of the low formic acid pressure is reflected in the similarity of kinetic data obtained in Table 2 (formally gas phase HCOOH treatment) and Table 3 (formally surface intermediate HCOOH\* treatment) for the Cu(211) surface

<sup>3</sup> See footnote 2

**Table 2** Steady state methanol formation rates and selected surface coverages obtained from microkinetic analysis of isolated CO hydrogenation, isolated CO<sub>2</sub> hydrogenation and combined CO and CO<sub>2</sub> hydrogenation by using Gibbs free energies calculated with the RPBE functional illustrated in Fig. 1

Data set	[CO*] (ML)	[H*] (ML)	[HCOO*] (ML)	[*] (ML)	CO TOF (s <sup>-1</sup> )	CO <sub>2</sub> TOF (s <sup>-1</sup> )	H <sub>2</sub> TOF (s <sup>-1</sup> )	HCOOH TOF (s <sup>-1</sup> )	MeOH TOF (s <sup>-1</sup> )
CO hydrogenation:									
Cu(111)	4.6 × 10 <sup>-3</sup>	5.9 × 10 <sup>-3</sup>	- <sup>a</sup>	0.99	-7.0 × 10 <sup>-5</sup>	-	-1.4 × 10 <sup>-4</sup>	-	7.0 × 10 <sup>-5</sup>
Cu(211)	0.47	9.4 × 10 <sup>-2</sup>	-	0.38	-2.7 × 10 <sup>-1</sup>	-	-5.4 × 10 <sup>-1</sup>	-	2.7 × 10 <sup>-1</sup>
CuZn(211)	0.49	9.9 × 10 <sup>-2</sup>	-	0.40	-6.4 × 10 <sup>-1</sup>	-	-1.3 × 10 <sup>0</sup>	-	6.4 × 10 <sup>-1</sup>
CO <sub>2</sub> Hydrogenation ( <i>Analysis 1</i> ) <sup>b</sup> :									
Cu(111)	-	5.9 × 10 <sup>-3</sup>	1.1 × 10 <sup>-4</sup>	0.99	-	-1.2 × 10 <sup>-1</sup>	-1.2 × 10 <sup>-1</sup>	1.2 × 10 <sup>-1</sup>	-4.7 × 10 <sup>-14</sup>
Cu(211)	-	1.5 × 10 <sup>-2</sup>	0.93	6.0 × 10 <sup>-2</sup>	-	-2.8 × 10 <sup>-2</sup>	-2.8 × 10 <sup>-2</sup>	2.8 × 10 <sup>-2</sup>	-9.5 × 10 <sup>-9</sup>
CuZn(211)	-	1.9 × 10 <sup>-3</sup>	0.99	8.0 × 10 <sup>-3</sup>	-	-2.0 × 10 <sup>-3</sup>	-2.0 × 10 <sup>-3</sup>	2.0 × 10 <sup>-3</sup>	-1.1 × 10 <sup>-12</sup>
CO <sub>2</sub> Hydrogenation ( <i>Analysis 2</i> ) <sup>b</sup> :									
Cu(111)	-	5.9 × 10 <sup>-3</sup>	1.1 × 10 <sup>-4</sup>	0.99	-	-6.0 × 10 <sup>-7</sup>	-1.8 × 10 <sup>-6</sup>	5.6 × 10 <sup>-9</sup>	6.0 × 10 <sup>-7</sup>
Cu(211)	-	1.5 × 10 <sup>-2</sup>	0.93	6.0 × 10 <sup>-2</sup>	-	-2.5 × 10 <sup>-5</sup>	-7.5 × 10 <sup>-5</sup>	2.0 × 10 <sup>-7</sup>	2.5 × 10 <sup>-5</sup>
CuZn(211)	-	1.9 × 10 <sup>-3</sup>	0.99	8.0 × 10 <sup>-3</sup>	-	-1.4 × 10 <sup>-5</sup>	-4.2 × 10 <sup>-3</sup>	1.4 × 10 <sup>-7</sup>	1.4 × 10 <sup>-5</sup>
Combined CO and CO <sub>2</sub> Hydrogenation ( <i>Analysis 1</i> ) <sup>b</sup> :									
Cu(111)	4.6 × 10 <sup>-3</sup>	5.9 × 10 <sup>-3</sup>	1.1 × 10 <sup>-4</sup>	0.99	-7.0 × 10 <sup>-5</sup>	-1.2 × 10 <sup>-1</sup>	-1.2 × 10 <sup>-1</sup>	1.2 × 10 <sup>-1</sup>	7.0 × 10 <sup>-5</sup>
Cu(211)	6.8 × 10 <sup>-2</sup>	1.4 × 10 <sup>-2</sup>	0.86	5.6 × 10 <sup>-2</sup>	-5.6 × 10 <sup>-3</sup>	-2.4 × 10 <sup>-2</sup>	-3.5 × 10 <sup>-2</sup>	2.4 × 10 <sup>-2</sup>	5.6 × 10 <sup>-3</sup>
CuZn(211)	9.6 × 10 <sup>-3</sup>	1.9 × 10 <sup>-3</sup>	0.98	7.9 × 10 <sup>-3</sup>	-2.4 × 10 <sup>-4</sup>	-2.0 × 10 <sup>-3</sup>	-2.4 × 10 <sup>-3</sup>	2.0 × 10 <sup>-3</sup>	2.4 × 10 <sup>-4</sup>
Combined CO and CO <sub>2</sub> hydrogenation ( <i>Analysis 2</i> ) <sup>b</sup> :									
Cu(111)	4.6 × 10 <sup>-3</sup>	5.9 × 10 <sup>-3</sup>	1.1 × 10 <sup>-4</sup>	0.99	-7.5 × 10 <sup>-5</sup>	-6.1 × 10 <sup>-7</sup>	-1.4 × 10 <sup>-4</sup>	6.1 × 10 <sup>-9</sup>	7.0 × 10 <sup>-5</sup>
Cu(211)	6.8 × 10 <sup>-2</sup>	1.4 × 10 <sup>-2</sup>	0.86	5.6 × 10 <sup>-2</sup>	-5.6 × 10 <sup>-3</sup>	-9.0 × 10 <sup>-8</sup>	-1.1 × 10 <sup>-2</sup>	8.3 × 10 <sup>-10</sup>	5.6 × 10 <sup>-3</sup>
CuZn(211)	9.6 × 10 <sup>-3</sup>	1.9 × 10 <sup>-3</sup>	0.98	7.9 × 10 <sup>-3</sup>	-2.6 × 10 <sup>-4</sup>	-1.4 × 10 <sup>-5</sup>	-5.2 × 10 <sup>-4</sup>	1.4 × 10 <sup>-7</sup>	2.6 × 10 <sup>-4</sup>

Gibbs free energies calculated [9] at 500 K,  $P_{H_2} = 40$  bar,  $P_{CO} = P_{CO_2} = 10$  bar and  $P_{MeOH} = P_{H_2O} = 1$  bar. A negative rate indicates consumption of the particular species

<sup>a</sup> Species not considered in mechanism

<sup>b</sup> *Analysis 1* data is obtained with 0 bar pressure for gas phase formic acid specified in the analyses, while *Analysis 2* data is obtained by specifying a pressure for gas phase formic acid corresponding to a production of formic acid at steady state of ~1 % of the methanol produced from CO<sub>2</sub> consumption

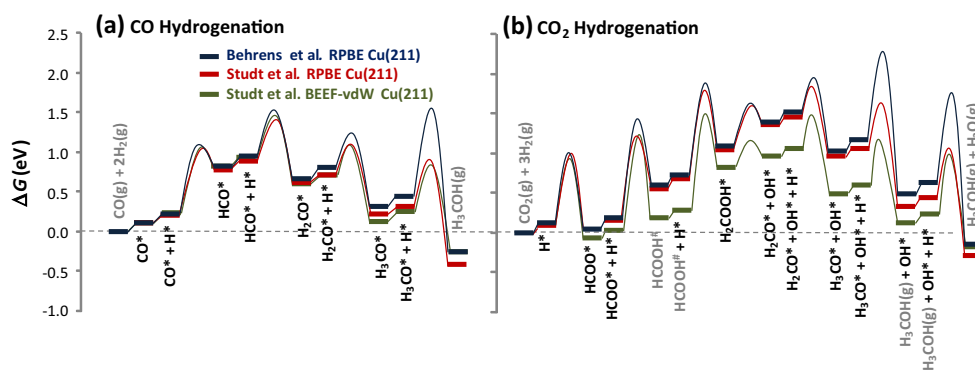


**Fig. 2** Comparative Gibbs free energy (See Footnote 1) profiles (500 K,  $P_{H_2} = 40$  bar,  $P_{CO} = P_{CO_2} = 10$  bar and  $P_{MeOH} = P_{H_2O} = 1$  bar) for CO and CO<sub>2</sub> hydrogenation on the Cu(211)

complete analysis of factors influencing methanol formation, compared to direct evaluation of the separate DFT energy profiles. For these combined microkinetic analyses (Table 2, *Analysis 1*) the methanol (only produced from CO) formation rates for the Cu(211) and CuZn(211) surfaces are now significantly slower compared to the corresponding methanol formation rates for isolated CO hydrogenation. This reflects the poisoning effect of high formate coverage (vide infra) on the surfaces, significantly inhibiting methanol formation from CO due to inhibition of CO surface concentration at steady state. For more realistic <sup>4</sup> *Analysis 2* of combined CO and CO<sub>2</sub> hydrogenation, in which the reincorporation of formic acid to yield methanol is facilitated, the slower methanol yield from CO<sub>2</sub> is reflected in the fact that the consumption rates of CO effectively correspond to the overall formation rate of methanol. However, these CO consumption rates are still significantly controlled by the availability of surface sites for CO adsorption on Cu(211) and CuZn(211), which are dominated by formate coverages of 0.86 and 0.98 ML, respectively. *Analysis 2* for combined CO and CO<sub>2</sub> hydrogenation results in a surface reactivity trend of Cu(211) > CuZn(211) > Cu(111), similar to the trend found for isolated CO<sub>2</sub> hydrogenation (*Analysis 2*). This is not in complete agreement with previous predictions [9] that favour methanol formation for CuZn(211) over Cu(211) based on direct interpretation of DFT energy profiles. Also, dominant CO selectivity for methanol formation on all three surfaces is reflected in the relative CO and CO<sub>2</sub> consumption rates, yielding CO selectivities of 100, 100 and 94 % for Cu(111), Cu(211) and CuZn(211), respectively. The microkinetic analyses show that factors related to poisoning effects of formate intermediates and CO/CO<sub>2</sub> selectivity towards methanol are not fully

accounted for when a direct interpretation of the DFT Gibbs free energy profiles is made.

surface as reported by Behrens et al. [9] and Studt et al. [10]. \*represents adsorbed states; #denotes HCOOH(g) for Behrens data and HCOOH\* for Studt data

accounted for when a direct interpretation of the DFT Gibbs free energy profiles is made.

The predominant selectivity for hydrogenation of CO, rather than CO<sub>2</sub>, for methanol formation observed in the above microkinetic analyses is in contrast to experimental observation that CO<sub>2</sub> is preferentially hydrogenated to methanol [18, 19] during Cu-catalyzed methanol synthesis. Studt et al. [10] notes that DFT-calculated free energy profiles for hydrogenation of CO<sub>2</sub> are usually found to involve intermediates and reaction barriers that are higher in energy when compared to CO hydrogenation [9, 11]. They investigated this discrepancy by recalculating the Cu(211) DFT data reported by Behrens et al. [9] with the newly developed BEEF-vdW functional [20]. From comparison of the RPBE and BEEF-vdW calculated Gibbs free energy diagrams the authors report [10] no significant changes in the respective energy profiles for CO hydrogenation. However, the free energies of most intermediates and transition states for CO<sub>2</sub> hydrogenation are found to be stabilized by up to 0.5 eV for BEEF-vdW relative to the RPBE data. This results in the highest free energy state for CO<sub>2</sub> hydrogenation to become comparable to the highest free energy state for CO hydrogenation for the BEEF-vdW data. Based on the direct interpretation of these BEEF-vdW derived Gibbs free energy profiles on Cu(211), Studt et al. [10] suggests that the use of BEEF-vdW will result in a qualitatively correct description of selectivity of CO<sub>2</sub> compared to CO hydrogenation for methanol formation.

Figure 2 illustrates the comparative RPBE-derived Gibbs free energy profiles for CO and CO<sub>2</sub> hydrogenation to methanol on Cu(211) reported by Behrens et al. [9] and Studt et al. [10], as well as the corresponding BEEF-vdW derived profiles [10], on the same graphs. Differences in the RPBE-derived Gibbs free energy profiles in Fig. 2 (red and blue profiles) are noticeable, e.g. for hydroxy, methoxy and formate hydrogenation barriers and gas versus adsorbed states of formic acid in the

<sup>4</sup> See Footnote 2

**Table 3** Steady state methanol turnover frequencies (TOF's) and coverages of selected surface intermediates for isolated CO hydrogenation, isolated CO<sub>2</sub> hydrogenation and combined CO and CO<sub>2</sub> hydrogenation mechanisms on Cu(211) from RPBE and BEEF-vdW Gibbs free energies illustrated in Fig. 2

Data set	[CO*] (ML)	[H*] (ML)	[HCOO*] (ML)	[HCOOH*] (ML)	[*] (ML)	CO TOF (s <sup>-1</sup> )	CO <sub>2</sub> TOF (s <sup>-1</sup> )	H <sub>2</sub> TOF (s <sup>-1</sup> )	MeOH TOF (s <sup>-1</sup> )
Studt et al. RPBE:									
CO	0.37	0.24	<sup>a</sup>	–	0.39	$-3.0 \times 10^0$	–	$-5.9 \times 10^0$	$3.0 \times 10^0$
CO <sub>2</sub>	–	$3.6 \times 10^{-2}$	0.90	$5.2 \times 10^{-5}$	$5.9 \times 10^{-2}$	–	$-7.9 \times 10^{-5}$	$-2.3 \times 10^{-4}$	$7.9 \times 10^{-5}$
CO + CO <sub>2</sub>	$5.4 \times 10^{-2}$	$3.4 \times 10^{-2}$	0.86	$4.9 \times 10^{-5}$	$5.6 \times 10^{-2}$	$-6.1 \times 10^{-2}$	$-7.1 \times 10^{-5}$	$-1.2 \times 10^{-1}$	$6.1 \times 10^{-2}$
Studt et al. BEEF-vdW:									
CO	0.29	0.23	–	–	0.48	$-8.8 \times 10^{-1}$	–	$-1.8 \times 10^0$	$8.8 \times 10^{-1}$
CO <sub>2</sub>	–	$1.9 \times 10^{-3}$	0.98	$1.8 \times 10^{-2}$	$3.9 \times 10^{-3}$	–	$-2.3 \times 10^{-4}$	$-6.9 \times 10^{-4}$	$2.3 \times 10^{-4}$
CO + CO <sub>2</sub>	$2.4 \times 10^{-2}$	$1.9 \times 10^{-3}$	0.97	$1.8 \times 10^{-2}$	$3.9 \times 10^{-3}$	$-5.8 \times 10^{-5}$	$-2.3 \times 10^{-4}$	$-8.1 \times 10^{-4}$	$2.9 \times 10^{-4}$

Gibbs free energies calculated [9] at 500 K,  $P_{H_2} = 40$  bar,  $P_{CO} = P_{CO_2} = 10$  bar and  $P_{MeOH} = P_{H_2O} = 1$  bar

<sup>a</sup> Species not considered in mechanism

profiles.<sup>5</sup> Nevertheless, the different RPBE data sets exhibit comparable Cu(211) steady state microkinetic results, which is evident upon comparing the results in Table 2 (considering isolated CO hydrogenation and *Analysis 2* data<sup>6</sup> for isolated CO<sub>2</sub> and combined CO/CO<sub>2</sub> hydrogenation) and Table 3. Therefore, only the Studt et al. [10] RPBE and BEEF-vdW data will be considered for microkinetic comparisons in the remainder of this letter as summarized in Table 3.<sup>7</sup>

Despite the similarities in the RPBE and BEEF-vdW free energies of intermediates and transition states (red and green profiles) for *isolated CO hydrogenation* in Fig. 2a, the RPBE methanol formation rate is more than three times faster than the BEEF-vdW methanol formation rate. This is again a reflection of the sensitivity of the kinetics to CO and H<sub>2</sub> adsorption energies, which are slightly less favourable for BEEF-vdW (i.e. 0.12 eV/CO\* and 0.12 eV/H\*) compared to RPBE (i.e. 0.10 eV/CO\* and 0.10 eV/H\*) and also explains the relatively lower CO\* coverage for BEEF-vdW. In contrast to this, comparison of the methanol formation rates (Table 3) for *isolated CO<sub>2</sub> hydrogenation* from the RPBE and BEEF-vdW energies (red and green profiles) in Fig. 2b shows that the methanol formation rate for BEEF-vdW is only about three times faster compared to RPBE, despite substantial differences in the DFT energy profiles. It should be noted, however, that for both functionals the isolated CO methanol formation rates are faster than the corresponding isolated CO<sub>2</sub> methanol formation rates by at least three orders of magnitude. The BEEF-vdW methanol formation rate for *combined CO and CO<sub>2</sub> hydrogenation* is found to be two orders of magnitude slower than the corresponding RPBE methanol formation rate. This could be explained by the more severe suppression of CO hydrogenation participation in the combined CO and CO<sub>2</sub> methanol formation mechanism for the BEEF-vdW functional, caused by the higher formate steady state coverage of 0.97 ML for BEEF-vdW compared to 0.86 ML for RPBE. This is supported by the one order lower CO versus CO<sub>2</sub> consumption rate for BEEF-vdW, while for RPBE the CO consumption rate is three orders higher than the CO<sub>2</sub> consumption rate.

From the relative consumption rates for CO and CO<sub>2</sub> hydrogenation in Table 3, both in isolation and combined,

the selectivity for methanol formation may readily be determined. A comparison of *isolated* CO versus CO<sub>2</sub> hydrogenation consumption rates reveals that CO selectivity to methanol is well above 99.9 % for both RPBE and BEEF-vdW.<sup>8</sup> Whereas the relative RPBE consumption rate for CO and CO<sub>2</sub> hydrogenation in *combination* corresponds to a CO selectivity of 99.9 %, the corresponding BEEF-vdW CO selectivity for CO and CO<sub>2</sub> hydrogenation in combination is only 20.0 %. This leads to apparent confirmation of the conclusion by Studt et al. [10] that the BEEF-vdW functional provides for an improved description of CO/CO<sub>2</sub> selectivity for methanol formation compared to known experimental results. However, it may be argued that artificial suppression of CO hydrogenation participation in the mechanism, caused by overestimated high formate steady state coverage, is likely in the kinetic analyses. The steady state RPBE and BEEF-vdW formate coverages of 0.86 and 0.97 ML in Table 3, for combined CO and CO<sub>2</sub> hydrogenation, respectively, are significantly higher when compared to experimental formate saturation coverages determined from single crystal Cu surface treatments with either H<sub>2</sub> and CO<sub>2</sub> or formic acid at appropriate Langmuir exposures. In particular, it is established that for Cu(111) a maximum formate saturation coverage of 0.25 ML is found from X-ray photoelectron spectroscopy (XPS) [21], scanning tunneling microscopy (STM) [22] and temperature programmed desorption (TPD) [23] studies. For Cu(110) different formate saturation coverages are reported, ranging from 0.31 ML from thermal desorption mass spectroscopy (TDS) and XPS experiments<sup>9</sup> to 0.25 ML ( $\pm 0.05$  ML) from temperature programmed desorption (TPD) studies [24]. For Cu(100) a microkinetic model based on experimental data predicts respective coverages of 0.33 and 0.07 ML for hydrogen and formate at high pressure (50 bar total pressure for H<sub>2</sub> and CO<sub>2</sub>) with empty sites predominating with a coverage of 0.52 ML [25]. Therefore, although to the best of our knowledge no experimental data for formate saturation coverage on the Cu(211) surface is available, it is reasonable to assume that the formate saturation coverage limit on Cu(211) will be significantly lower than the steady state coverages reported from the microkinetic analyses in Table 3.

In an attempt to investigate the effect of formate saturation coverage on both the rate of methanol formation and CO/CO<sub>2</sub> selectivity, a microkinetic analysis was performed for *isolated* CO<sub>2</sub> and *combined* CO and CO<sub>2</sub> hydrogenation

<sup>5</sup> See details as discussed in the Supplementary Material of both Refs. [9] and [10]

<sup>6</sup> *Analysis 2* data in Table 2 is considered to be more appropriate than the data corresponding to *Analysis 1* for this comparison to the results in Table 3, because of the artificial omission of any formic acid pressure in *Analysis 1*. See Footnote 2 for more details

<sup>7</sup> Note that for these energy profiles and microkinetic analyses no gas phase formation of formic acid is considered, but rather the formation of surface intermediate HCOOH\*, effectively eliminating the possibility for formic acid to form as a product.

<sup>8</sup> See Footnote 7

<sup>9</sup> The 0.31 ML formate saturation coverage was calculated from the  $3.4 \times 10^{14}$  formates/cm<sup>2</sup> coverage [reported by Henn FC, Rodriguez JA, Campbell CT (1990) Surf. Sci. 236:282] based on a Cu(110) (1 × 1) surface unit cell with dimensions  $a = 3.6147 \text{ \AA}$  and  $b = 2.5560 \text{ \AA}$ .

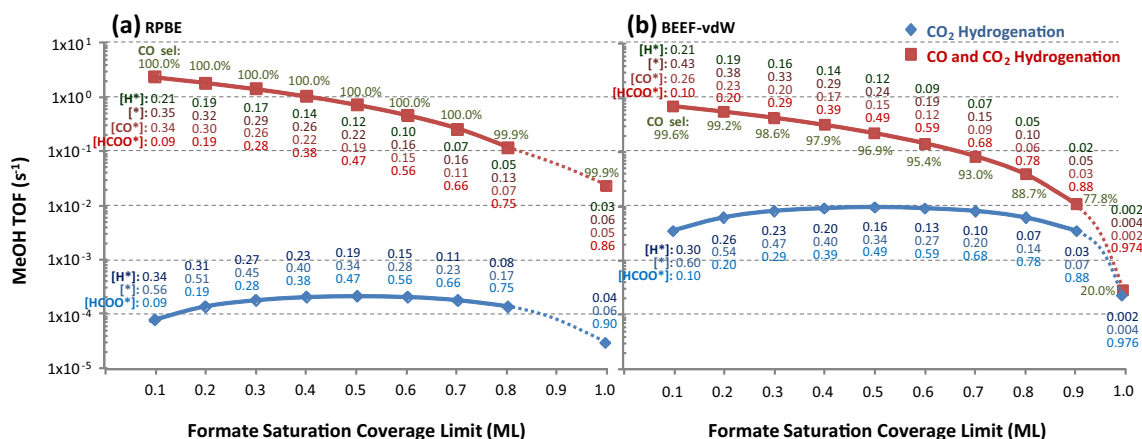


**Fig. 3** Relative steady state methanol formation rates (logarithmic scale) on the Cu(211) surface as a function of formate saturation coverage limit (see Footnote 10). Both isolated CO<sub>2</sub> hydrogenation and combined CO and CO<sub>2</sub> hydrogenation mechanisms utilize Gibbs free energy DFT data from Studt et al.[10]: **a** RPBE and **b** BEEF-vdW. The labels on the graphs display calculated steady state

coverage data for selected surface species, as well as the CO selectivity (%) for methanol formation during combined CO and CO<sub>2</sub> hydrogenation, at the corresponding formate saturation limit. The data extrapolated to 1.0 ML saturation coverage limit corresponds to the kinetic analyses in Table 3

for both the RPBE and BEEF-vdW derived free energy data by considering a range of formate saturation coverage limits ranging from 0.1 to 0.8 ML and 0.1 to 0.9 ML for RPBE and BEEF-vdW, respectively.<sup>10</sup> Figure 3 illustrates the methanol formation rates for the four scenarios as a function of formate saturation coverage limit.

From Fig. 3 it is evident that upon lowering formate saturation coverage limits, the methanol formation rates from isolated CO<sub>2</sub> hydrogenation (blue traces) are significantly faster for both BEEF-vdW and RPBE compared to the rates in Table 3 (corresponding to the rates at formate saturation coverage limit of 1.0 ML on the respective graphs). The BEEF-vdW CO<sub>2</sub> hydrogenation methanol formation rates are found to be consistently faster than the corresponding RPBE rates by more than an order of magnitude over the whole formate saturation coverage limit range, in qualitative agreement with the conclusion by Studt et al. [10]. The maximum methanol formation rates for isolated CO<sub>2</sub> hydrogenation are found at a formate saturation coverage limit of 0.5 ML and are  $2.2 \times 10^{-4}$  and  $1.0 \times 10^{-2} \text{ s}^{-1}$  for

<sup>10</sup> The formate saturation coverage limit is defined as the sum of the saturation coverage limit of HCOO\* and HCOOH\* on the surface. It is found that HCOOH\* constitutes at most only 0.02 ML of the combined total coverage, effectively implying that the steady state coverage for these two species is mainly due to HCOO\* on the surface. For the RPBE functional a saturation coverage limit range of 0.1–0.8 ML was considered, because it is evident from the RPBE steady state formate coverage for combined CO and CO<sub>2</sub> hydrogenation in Table 3 that the highest coverage of 0.86 ML obtained represents an upper limit for formate coverage. Similarly, for the BEEF-vdW functional a saturation coverage limit of 0.1–0.9 ML was considered because the upper limit for formate saturation coverage approaches 0.97 ML (Table 3). See Supplementary Material for more details

RPBE and BEEF-vdW, respectively. In an effort to gain insight into the increased rates at 0.5 ML formate saturation coverage, degree of rate control sensitivity analysis for both functionals at 0.5 and 1.0 ML formate saturation coverage was performed.<sup>11</sup> In all analyses it was consistently found, however, that the rate determining step is the hydrogenation of formic acid. This indicates that the increased methanol formation rates at lower formate saturation coverage limits are not caused by changes in the rate determining step of CO<sub>2</sub> hydrogenation. It should be noted that these methanol formation rates for both functionals are still significantly slower than the methanol formation rates from isolated CO hydrogenation (Table 3).

The methanol formation rates for combined CO and CO<sub>2</sub> hydrogenation in Fig. 3 (red traces) are found to steadily increase for both functionals upon lowering of the formate saturation coverage limits. This may be explained by the increased coverage of CO\* (also shown in Fig. 3) upon increased availability of surface sites, effectively allowing the faster CO hydrogenation mechanism to increasingly contribute to methanol formation. It is noticeable that BEEF-vdW methanol formation rates are consistently three times slower than the corresponding RPBE rates over the formate saturation coverage limit range below 1.0 ML. For example, at

coverage data for selected surface species, as well as the CO selectivity (%) for methanol formation during combined CO and CO<sub>2</sub> hydrogenation, at the corresponding formate saturation limit. The data extrapolated to 1.0 ML saturation coverage limit corresponds to the kinetic analyses in Table 3

<sup>11</sup> The procedure, based on the methods described by (a) Saltelli A, Ratto M, Tarantola S, Campolongo F (2012) Chem. Rev. 112:PR1 and (b) Stegelmann C, Anfreasen A, Campbell CT (2009) J. Am. Chem. Soc. 131:8077, involved isolated increase of each of the seven barriers in the CO<sub>2</sub> hydrogenation reaction sequence by 0.1 eV in each case determining the methanol formation rate at steady state. Four sets of data were obtained for each of the RPBE and BEEF-vdW determined DFT data sets at 0.5 and 1.0 ML formate saturation coverage limit, respectively



0.5 ML formate saturation coverage limit the BEEF-vdW methanol formation rate is  $2.3 \times 10^{-1} \text{ s}^{-1}$  compared to the corresponding RPBE rate of  $7.4 \times 10^{-1} \text{ s}^{-1}$ . A comparison of CO methanol selectivities for the RPBE and BEEF-vdW data is also included in Fig. 3 as a function of formate saturation coverage limit. For RPBE, methanol is exclusively produced from CO over the whole formate saturation coverage limit range, while the CO selectivity for BEEF-vdW rapidly increases from 20.0 % at 1.0 ML formate saturation coverage limit to 99.6 % at 0.1 ML formate saturation coverage limit. Given that experimental studies on single Cu crystal surfaces show formate saturation coverages to be lower than 0.31 ML [21–25]<sup>12</sup> (vide supra), it is reasonable to assume that an upper limit for the saturation coverage of formate on Cu(211) will not exceed 0.5 ML. At 0.5 ML formate saturation coverage limit it follows from Fig. 3 that the RPBE and BEEF-vdW energy data will represent CO selectivities to methanol of 100.0 and 96.9 %, respectively. Although these results do suggest a slight increase in selectivity of CO<sub>2</sub> upon making use of the BEEF-vdW data in the microkinetic analysis, it is evident that CO selectivity to methanol will still dominate both the RPBE and BEEF-vdW calculated mechanisms at more realistic formate coverages, in contrast to the conclusions made from direct interpretation of the respective DFT-derived Gibbs free energy profiles [10].

In conclusion, the direct interpretation of DFT-derived Gibbs free energy profiles for Cu-catalyzed methanol synthesis in literature was investigated by conducting probing mean field microkinetic analyses. In particular, it was reported by Behrens et al [9] that experimental methanol formation reactivity trends may be correlated to DFT energy profiles on model catalyst surfaces yielding the following reactivity trend for both CO and CO<sub>2</sub> hydrogenation to methanol: CuZn(211) > Cu(211) > Cu(111). Microkinetic analyses confirmed the lowest reactivity of the Cu(111) surface for methanol formation. However, methanol formation rates on Cu(211) and CuZn(211), although of similar orders of magnitude, were the highest on CuZn(211) for isolated CO hydrogenation, but the highest on Cu(211) for isolated CO<sub>2</sub> hydrogenation, as well as combined CO and CO<sub>2</sub> hydrogenation. It is concluded that the direct interpretation of DFT energy profiles, and subsequent attempts to correlate this with experimental observations, are hampered by the high coverage poisoning effect of formate intermediates and the prediction of CO/CO<sub>2</sub> selectivity trends. In a subsequent study, Studt et al. [10] reported that a new DFT functional, BEEF-vdW, can correctly account for CO/CO<sub>2</sub> selectivities during Cu-catalysed methanol synthesis. However, a comparative microkinetic analysis of the RPBE versus BEEF-vdW DFT-reported energy profiles revealed that CO selectivity for methanol formation remains

dominant for both functionals upon consideration of saturation coverage limit effects for formate intermediates.

In general, the current letter serves to highlight the importance of applying a microkinetic analysis when DFT data is interpreted as this allows for the subtle influence of coverage and saturation effects of surface intermediates on catalytic rates to be accounted for. It should be noted that expansion of the DFT mechanistic schemas for Cu-catalyzed methanol synthesis could lead to significantly improved microkinetic interpretations of methanol synthesis catalysis. In particular, both the number and nature of elementary steps, e.g. inclusion of elementary steps for the water–gas-shift (WGS) reaction for correct description of CO/CO<sub>2</sub> selectivity, as well as the definition of interaction between terraces and steps on the model catalyst surfaces, needs to be considered to ensure an appropriate DFT data set for robust kinetic model developments.

**Acknowledgement** Prof Eric van Steen (University of Cape Town) is acknowledged for his inputs and proof reading of the manuscript.

## References

1. Lee S (1989) Methanol Synthesis Technology. CRC Press, Boca Raton
2. Olah GA, Goeppert A, Prakash GKS (2009) Beyond Oil and Gas: The Methanol Economy, 2nd edn. Weinheim, Wiley-VCH
3. Mei D, Xu L, Henkelman G (2009) J Phys Chem 313:4522
4. Yang Y, Evans J, Rodriguez JA, White MG, Liu P (2010) Phys Chem Chem Phys 12:9909
5. Chuasiripattana K, Warschkow O, Delley B, Stampfl C (2010) Surf Sci 604:1742
6. Zhao Y-F, Yang Y, Mims C, Peden CHF, Li J, Mei D (2011) J Catal 281:199
7. Yang Y, White MG, Liu P (2012) J Phys Chem C 116:248
8. Zhao Y-F, Rousseau R, Li J, Mei D (2012) J Phys Chem C 116:15952
9. Behrens M, Studt F, Kasatkin I, Kühn S, Hävecker M, Abild-Pedersen F, Zander S, Girgsdies F, Kurr P, Knip B-L, Tovar M, Fischer RW, Nørskov JK, Schlögl R (2012) Science 336:893
10. Studt F, Abild-Pedersen F, Varley JB, Nørskov JK (2013) Catal Lett 143:71
11. Grabow LC, Mavrikakis M (2011) ACS Catal. 1:365
12. Studt F, Abild-Pedersen F, Wu Q, Jensen AD, Temel B, Grunwaldt J-D, Nørskov JK (2012) J Catal 293:51
13. Medford AJ, Sehested J, Rossmeisl J, Chorkendorff I, Studt F, Nørskov JK, Moses PG (2014) J Catal 309:397
14. Studt F, Sharafutdinov I, Abild-Pedersen F, Elkjær CF, Hummelshøj JS, Dahl S, Chorkendorff I, Nørskov JK (2014) Nature Chem. doi:10.1038/NCHEM.1873
15. Dumesic JA, Rudd DF, Aparicio LL, Rekoske JE (1993) Trevino AA *The Microkinetics of heterogeneous Catalysis*. American Chemical Society, Washington, DC
16. Van Helden P, van den Berg J-A, Weststrate CJ (2012) ACS Catal. 2:1097
17. Yoshihara J, Campbell CT (1996) J Catal 161:776
18. Hansen JB, Nielsen PEH (2008) In: Ertl G, Knözinger H, Schüth F, Weitkamp J (eds) Handbook of heterogeneous catalysis. Wiley, Weinheim

<sup>12</sup> See Footnote 9

19. Chinchen GC, Denny PJ, Parker DG, Spencer MS, Whan DA (1987) *Appl. Catal.* 30:333
20. Wellendorf J, Lundgaard KT, Møgelhøj A, Petzold V, Landis DD, Nørskov JK, Bligaard T, Jacobsen KW (2012) *Phys. Rev. B* 85:235149
21. Nakamura J, Kushida Y, Choi Y, Uchijima T, Fujitani T (1997) *Vac Sci Technol A* 15:1568
22. Fujitani T, Choi Y, Sano M, Kushida Y, Nakamura J (2000) *J. Phys. Chem. B* 104:1235
23. Yatsu T, Nishimura H, Fujitani T, Nakamura J (2000) *J Catal* 191:423
24. Hayden BE, Prince K, Woodruff DP, Bradshaw AM (1983) *Surf Sci* 133:589
25. Rasmussen PB, Holmblad PM, Askgaard T, Oveson CV, Stoltze P, Nørskov JK, Chorkendorff I (1994) *Catal Lett* 26:373